Structural, Vibrational and Electronic Properties with Pharmacokinetics, Drug-likeness, and Molecular Docking of Furandimethanol

Madhab Raj Bhatt*, Govind Bahadur Dhami, Shiv Raj Joshi

Department of Physics, Siddhanath Science Campus, Mahendranagar, Kanchanpure, Tribhuvan University, Nepal

Research Article

ISSN: 3059-9504 (online)
DOI: https://doi.org/10.3136/ajs.v2i1.87746

Article History

Received: September 20, 2025; Revised: October 22, 2025; Accepted: October 29, 2025; Published: December 25, 2025

Keywords

Density functional theory, BHMF, HOMO-LUMO, MESP, UV-Vis, Molecular Docking, Pharmacokinetics, Drug-likeness.

***Corresponding author**

Email: phy.madhab@gmail.com (MR Bhatt)

ABSTRACT

In this study, geometrical parameters, electronic and vibrational properties of furandimethanol (BHMF) have been analyzed by using density functional theory (DFT) at B3LYP/6-31g level. Forty-five normal modes of vibration were obtained and analyzed with their potential energy contributions. The calculated Raman and IR spectra were plotted using scaled wavenumbers. Molecular electrostatic potential surface (MESP), ultraviolet visible (UV-Vis) spectra and Mulliken charges were mapped to understand electronic properties. Swiss ADME web tool was used for prediction of physicochemical, pharmacokinetics, drug-likeness and medicinal properties of titled molecule. Molecular docking studies against 1S5B (2.13 Å resolution), a mutant cholera holotoxin from *Vibrio cholerae*, were performed using Autodock tools like BIOVIA Discovery Studio, PyMOL, Python and Open Babel. The molecular docking study indicates that the furandimethanol is moderate inhibitor of 1S5B.

1. INTRODUCTION

In recent time, a majority of researchers are using computational tools widely used in chemistry to investigate real problems in chemical, pharmaceutical, biotechnology, and material science. They use the results of theoretical calculations, to calculate the structure and properties of molecules and solid materials both in physics and chemistry [1]. Computational chemistry and computational physics are used in the designing of new drugs and materials to solve numerical problems. Nowadays, researchers use various computational programs to predict the molecular structure and physical properties of bioactive molecules [2]. The density functional theory (DFT) is a popular method for defining the structural and electronic properties of atoms and molecules [3]. Furandimethanol, commonly known as 2,3–Bis(hydroxymethyl)furan (BHMF), IUPAC name Furan-2,3-diyl)dimethanol, is a heterocyclic organic compound with oxygen as hetero member. It is a water-soluble furan carrying two hydroxymethyl substituents at the 2-and 3-position and is a member of diol. It is produced from cellulose and has received attention as a bio-feedstock. Its commercial samples can appear yellowish or tan [4]. The Optimized structure of Furandimethanol is presented in Fig. 1.

Compounds classified as heterocyclic probably constitute the largest and most varied family of organic compounds. Among heterocyclic compounds, five-membered heterocycles constitute a wide and differentiated group with a broad spectrum of biological activity. Compounds from this class are present in nature as constituents of nucleic acid, so many important amino acids, alkaloids and hormones [4]. Joshi *et.al* have studied the structure, MESP and HOMO-LUMO of 10-acetyl-10H-phenothiazine-5-oxide using vibrational spectroscopy quantum chemical method [5]. Yadav *et.al* have studied on *ab Initio* and DFT study of HCN: Role of temperature for the formation of HCN molecule in the interstellar medium [6].

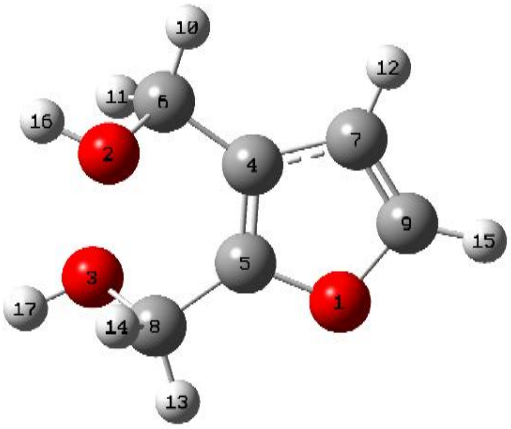

Fig. 1: Optimized Structure of Furandimethanol.

Pharmacokinetics is the branch of pharmacology that deals with the study of what the body does to a drug, summarized by ADME (Absorption, Distribution, Matabolism, Excreation). It focuses at how a drug enters the bloodstream through absorption, how it spreads to tissues and organs through distribution, how the body's enzymes break it down through metabolism, and how it is removed from the body through excretion in urine, bile, or sweat. Drug-likeness is a measure which ensures whether a chemical compound become an effective, safe, and orally active drug in humans.

Molecular docking approach is a computer-aided technique to predict protein-ligand interaction of a drug molecule. It predicts biding modes as well as binding affinity of ligand with target proteins which plays key role in drug design [7,8].

2. METHODOLOGY

Taking initial molecular data available from PubChem database [9], geometry optimization was performed. Taking the optimized parameters, the vibrational spectra were calculated by using B3LYP/6-31g [10, 11], level of theory employing Gaussian 09 program [12] without any constraints on the geometry of molecule [13]. Using the same level of theory, geometrical parameters bond lengths, bond angles and dihedral angles were calculated. The basis set used for the calculations is based on Becke's three-parameter (local, non-local, Hartree-Fock) hybrid exchange functional with Lee-Yang-Parr correlation Functional (B3LYP) [10,11,14, 15].

As the second task, normal modes of vibration and their corresponding Raman activities and IR intensities were calculated by the program Gar2Ped [16]. All the 45 normal modes of vibrations were assigned with their potential energy contributions using internal coordinates recommended by Pulley [17]. The visualization of calculated data is done by using the Gauss View [17].

Raman spectra and IR spectra were plotted using OriginPro 7 programme, UV-visible spectra and molecular electrostatic surface potential (MESP) were plotted using Gauss view. Mulliken atomic charges were plotted using Microsoft excel. Swiss ADME web tool [18] is utilized for prediction of physicochemical, pharmacokinetics, drug-likeness and medicinal chemistry properties of titled molecule. The canonical SMILES of the molecule were retrieved from the PubChem database [9] and fed into the Swiss ADME tool. This tool returns the full set of data including number of hydrogen bond acceptors, number of donors, molar refractivity, polar surface area (PSA), rotatable bonds, AlogP and other crucial parameters.Molecular docking studies were performed using AutoDock Vina [19], AutoDock tools [20], BIOVIA Discovery Studio [21], PyMOL [22], Python and Open Babel. Docking proteins were retrieved from the RCSB Protein Data Bank [23].

The target proteins were retrieved in PDB format from the RCSB Protein Data Bank and then were prepared using BIOVIA Discovery Studio, AutoDock Tools for final docking purpose. In the last step of preparation, polar hydrogen atoms were accurately attached to the target protein structure after deleting all water and unnecessary ligand molecules. The ligand, BHMF, was downloaded from the PubChem database in SDF format and then converted to PDB format using Open Babel [24]. It was prepared using AutoDock tools and saved in PDBQT format which was the same format as that of protein. The molecular docking technique was employed using blind docking, wherein the grid was designed optimally to cover the maximum possible binding sites of the protein. AutoDock Vina was executed to perform molecular docking after the detailed preparation of the protein, ligand, and configuration file. The docking process was initiated using the Vina command, ensuring a precise and systematic approach to the analysis.

The scoring function for AutoDock Vina can be obtained using the following equation

$$\Delta G_{binding} = \Delta G_{H-bond} + \Delta G_{hydrophobic} + \Delta G_{repulsion} + \Delta G_{gauss} + \Delta G_{AutoDock\ Vina\ score} \quad (i)$$

where, ΔG_{H-bond} represents the change in the binding energy due to hydrogen bond, $\Delta G_{hydrophobic}$, due to hydrophobic interaction, due to steric effect, $\Delta G_{repulsion}$(gauss^1 (d) = $e^{-(\frac{d}{0.5\text{Å}})^2}$, gauss^2(d) =$e^{-(\frac{d-3\text{Å}}{2\text{Å}})^2}$ and Repulsion(d) $= \begin{cases} d^2, & d < 0 \\ 0, & d \geq 0 \end{cases}$), due to repulsion and ΔGAutoDock Vina score, due to rotational bonds penalty.

The hydrophobic term equals 1, when d < 0.5 Å; 0, when d > 1.5 Å, and is linearly interpolated between these values. The hydrogen bonding term equals 1, when d < −0.7 Å; 0, when d > 0, and is similarly linearly interpolated in between X- score, we formally treat metals as hydrogen bond donors. In this implementation, all interaction functions $f_{t_i t_j}$ are cut off at r_{ij} = 8 Å (Trott and Olson, 2009)

The conformation-independent function g was chosen to be

$$g(C_{inter}) = \frac{C_{inter}}{1+wN_{rot}} \quad (ii)$$

Where, N_{rot} represents number of active rotatable bonds between heavy atoms in ligand and w is the associated weight.

Results obtained from AutoDock Vina were visualized and analyzed using PyMOL and BIOVIA Discovery Studio.

3. RESULTS AND DISCUSSION

3.1 Geometric parameters

The bond lengths, bond angles and dihedral angles are basic properties of molecules to deal with molecular geometry. In a molecule bond length is defined as the average distance between nuclei of two bonded atoms in it. The value of bond lengths varies from molecule to molecule as it depends upon various factors like types of atoms, orbital hybridization, electronic and steric nature of the substituents. The bond length, bond angle and dihedral angle data for title molecule is listed in Table 1 below:

Table1: Optimized values of Bond length, Bond angle and Dihedral angle.

Bond Length	Optimized value (Å)	Bond Angle	Optimized value (°)	Dihedral Angle	Dihedral angle (°)
O1-C5	1.359	C5-O1-C9	106.62	C9-O1-C5-C4	0
O1-C9	1.359	C6-O2-H16	106.93	C9-O1-C5-C8	-179.96
O2-C6	1.428	C8-O3-H17	106.91	C5-O1-C9-C7	-0.01
O2-H16	0.972	C5-C4-C6	127.11	C5-O1-C9-H15	179.99

O3-C8	1.429	C5-C4-C7	106.12	H16-O2-C6-C4	179.84
O3-H17	0.972	C6-C4-C7	126.77	H16-O2-C6-H10	59.19
C4-C5	1.376	O1-C5-C4	110.57	H16-O2-C6-H11	-58.74
C4-C6	1.474	O1-C5-C8	116.06	H17-O3-C8-C5	-179.88
C4-C7	1.415	C4-C5-C8	133.37	H17-O3-C8-H13	59.2
C5-C8	1.47	O2-C6-C4	107.91	H17-O3-C8-H14	-58.87
C6-H10	1.095	O2-C6-H10	108.52	C6-C4-C5-O1	-179.99
C6-H11	1.095	O2-C6-H11	108.73	C6-C4-C5-C8	-0.03
C7-C9	1.376	C4-C6-H10	111.24	C7-C4-C5-O1	0.01
C7-H12	1.081	C4-C6-H11	111.78	C7-C4-C5-C8	179.96
C8-H13	1.094	H10-C6-H11	108.58	C5-C4-C6-O2	90
C8-H14	1.094	C4-C7-C9	106.13	C5-C4-C6-H10	-151.07
C9-H15	1.08	C4-C7-H12	127.8	C5-C4-C6-H11	-29.51
		C9-C7-H12	126.07	C7-C4-C6-O2	-90
		O3-C8-C5	108.05	C7-C4-C6-H10	28.93
		O3-C8-H13	108.58	C7-C4-C6-H11	150.5
		O3-C8-H14	108.63	C5-C4-C7-C9	-0.01
		C5-C8-H13	111.37	C5-C4-C7-H12	-179.98
		C5-C8-H14	111.42	C6-C4-C7-C9	179.98
		H13-C8-H14	108.71	C6-C4-C7-H12	0.02
		O1-C9-C7	110.57	O1-C5-C8-O3	-90.05
		O1-C9-H15	115.63	O1-C5-C8-H13	29.12
		C7-C9-H15	133.8	O1-C5-C8-H14	150.7
				C4-C5-C8-C3	90
				C4-C5-C8-H13	-150.83
				C4-C5-C8-H14	-29.25
				C4-C7-C9-O1	0.01
				C4-C7-C9-O15	-179.99
				H12-C7-C9-O1	179.98
				H12-C7-C9-H15	-0.02

Generally, the C-C single bond length is 1.54Å, C-H is 1.09Å, C-O is 1.43Å and that of C=C 1.34Å [25]. But, in this study the longest C-C bond was found between C4-C6 with the value 1.474 Å and the shortest C-C bonds were found between C4-C5 and C7-C9 with the same value 1.376Å. The longest C-O bond wsa found between C8-O3 with the value 1.429Å the shortest C-O bonds were found between C9-O1 and C5-O1 with the same value 1.359Å. O-H bond length was found to be 0.972Å and C-H bond length was found in the range 1.080Å -1.095Å. The highest and lowest bond angles were found between C7-C9-H15 and C5-C4-C7 with respective values 133.80° and 106.12°. The dihedral angle is the clockwise angle between two planes, both of which pass through the same bond. Here, the lowest to highest dihedral angles in clockwise directiobs were found in the range 0.01°-179.96°, whereas the lowest to highest dihedral angles in counter-clockwise direction were found in the range 0.00°- 179.99°.

3.2 Vibrational Assignments

Furandimethanol (BHMF) consists of 17 atoms and hence it gives 45 fundamental modes of vibration which are both Raman and IR

active. A complete vibrational analysis of these fundamental vibrational modes was made by using DFT/ B3LYP/6-31g. Also, HF calculations were made using same level of basis set. The PED assignments were given as per the internal coordinate system. The calculated vibrational wavenumbers (in both B3LYP and HF), IR intensity, Raman activity and calculated PED for each normal mode are as shown in Table 2 and IR and Raman spectra are shown in Figs. 2 and 3, respectively.

Table 2: Vibrational wavenumbers (cm^{-1}), Raman activity (km/mol), IR Intensity ($Å^4$/a.m.u) and potential energy distribution.

Wavenumber			Raman Activity	IR Intensity	Potential Energy Distribution (PED)($\geq 5\%$)
Unscaled	Scaled				
DFT	DFT	HF			
49	49	86	0.5774	0.1069	R[υ(CO)](7)+τ(CC)(74)+τ(CO)(7)
94	95	151	0.7297	3.4596	R[υ(C=C)(15)+oop(CC(13)]+ τ(CC)(56)
158	159	216	2.6337	6.0628	R[oop(CC(44)+υ(CC)(15)+δ_{in}(CC)(6)]+δ(COC)(19)
188	189	258	1.9258	7.6907	R[oop(CC(50)+υ(CC)(9)+δ_{in}(CC)(6)]+δ(COC)(17)
237	238	274	1.6805	2.8936	R[δ_{in}(CC)(47)+oop(CC(7)]+υ(CO)(11)+τ(CC)(7)
255	256	343	9.7949	248.580	τ(CO)(92)
337	339	388	8.0452	9.5009	R[υ(CO)](7)+τ(CO)(73)+δ(COC)(12)
358	360	436	2.2902	0.2435	R[δ_{in}(CC)(55)+υ(C=C)(8)+oop(CC(6)]+ δ(COC)(12)
398	398	481	0.8150	11.8220	R[τ′(24)+δ_{in}(CC)(5)+oop(CC(5)]+ δ(COC)(30)
417	417	674	2.6919	1.9238	R[δ](13)+υ(CC)(15)+ oop(CC(11) + δ_{in}(CC)(5)] + δ(COC)(21) +υ(OH)(11)
620	620	711	2.6844	4.6294	R[τ](75)+τ′(9)]+ υ(CO)(6)
673	671	749	6.4752	13.0880	R[τ′(38) + oop(CC(23) +υ(CC)(17) +υ(CO)(6)]
693	691	790	0.2901	23.9430	R[δ(24)+τ′(6)+oop(CC(6)]+υ(CC)(19) +δ(COC)(25)+
734	731	822	3.158	39.6590	R[oop(CH)(27) + τ′(20) +υ(CO)(8)] +oop(CC(13) +υ(CC)(12) + δ(COC)(5)
765	762	887	2.7985	32.2000	R[oop(CH)(36)+τ′(15)+τ(10)+oop(CC(13)]+ υ(CO)(10)
888	883	983	0.9953	5.3747	R[oop(CH)(85) + υ(CO)(7) + τ(5)]
906	900	1046	3.8238	22.8930	R[δ′(57) + υ(CO)(19)]+ ρ(CH_2)(6)
967	960	1057	4.4108	9.3792	R[δ′(13) + υ(CO)(11) + δ(9) + υ(CC)(5)+ υ(C=C)(5)] + ρ(CH_2)(40)
971	964	1072	10.9727	43.3530	υ(CO)(75) + δ(COC)(5)
978	970	1111	6.4668	45.4380	υ(CO)(75) + ρ(CH_2)(5)
1007	999	1122	6.0460	3.7559	R[υ(CO)](5) +ρ(CH_2)(61) + υ(CO)(12)
1041	1033	1146	7.9910	4.3749	R[υ(CO)(65) + δ_{in}(CH)(19)]
1110	1099	1161	2.2426	7.7562	R[δ_{in}(CH)(14) + δ(8) +υ(CO)(14) +υ(CC)(7) + δ_{in}(CC)(7)] + ρ(CH_2)(34)
1161	1149	1219	14.0402	1161.20	R[δ_{in}(CH)](45)+υ(C=C)(12) +υ(CO)(17) +υ(CC)(10)]+ {ρ(7) + γ (6) }(CH_2)
1198	1185	1273	6.9571	7.0379	R[υ(CO) (22) + υ(CC)(26) + δ(10) +υ(C=C)(6)]+ γ(CH_2)(16)
1238	1224	1309	11.6332	26.4070	R[δ_{in}(CH)(12) + δ(7) + υ(CC)(5)] + δ(CHO)(27) + γ(CH_2)(19)+ υ(CC)(11)
1257	1242	1346	3.2808	36.5350	δ(CHO)(63) + ω(CH_2)(26)
1291	1275	1351	8.1630	54.4370	R[δ(5)] + δ(CHO)(36) + ω(CH_2)(26) + γ(CH_2)(17)+ υ(CC)(6)
1306	1290	1397	2.8531	1.3104	R[δ_{in}(CH)](43) + γ(CH_2)(40)
1321	1304	1469	19.8075	6.2351	R[υ(CC)(10) +υ(CO)(10)] + γ(CH_2)(63) +υ(CC)(5)
1419	1399	1516	4.5706	6.9053	R[υ(CC)(20)+δ_{in}(CH)(23)+υ(CO)(5)] +ω(CH_2)(21)
1473	1451	1555	9.8611	7.2197	ω(CH_2)(67) + δ(CHO)(17) + υ(CC)(5)
1478	1455	1568	18.6438	5.1138	R[υ(CC)](6)+ ω(CH_2)(44)+υ(CC)(18)+ δ(CHO)(14)
1507	1483	1640	81.2979	10.3620	R[υ(C=C)](63) + δ_{in}(CH)(17) +δ′(5)+ υ(CC)(5)
1545	1520	1652	24.1001	3.5611	δ(CH_2)(94)
1561	1535	1658	5.4589	7.1581	δ(CH_2)(96)
1655	1624	1765	26.1030	3.8103	R[υ(C=C)](66) +υ(CC)(14)]
3022	2900	3050	89.7099	59.2930	υ(CH_2)(100)

3040	2916	3088	114.072	40.3970	$\upsilon(CH_2)$(99)
3068	2941	3118	50.4533	27.4440	$\upsilon(CH_2)$(99)
3090	2961	3125	59.6634	16.7150	$\upsilon(CH_2)$(99)
3279	3132	3279	69.5059	2.1007	R[υ(CH)](99)
3326	3175	3332	112.266	0.2693	R[υ(CH)](99)
3458	3293	3519	242.713	5.4531	υ(OH)(98)
3463	3298	3656	234.425	3.3227	υ(OH)(99)

3.2.1 Furan ring vibration

Generally, C—H stretching occurs in the region 3100-3000 cm^{-1} [26]. In this study, C-H stretching was calculated at 3132cm^{-1} and 3175cm^{-1} with Raman activity/IR intensity 69.5059/112.2660 and 2.1007/0.2693 units respectively. C-H in plane bending vibrations were recorded at 1399cm^{-1}, 1290cm^{-1}, 1224cm^{-1}, 1099cm^{-1} and 1033cm^{-1} with Raman activity/IR intensity 4.5706/6.9053, 2.8531/1.3104, 11.6332/26.4070, 14.0403/1161.2000, 2.2426/7.7562 and 7.9910/4.3749 units respectively in scaled DFT. The out of plane bending was recorded below 883 cm^{-1}. The ring C-C stretching vibrations are found to be strong in the band from 1600cm^{-1}-1400cm^{-1}[26], here they were recorded at 1624cm^{-1}, 1455cm^{-1} and 1399cm^{-1} with Raman activity/IR intensity 26.1030/3.1803, 18.6438/5.1138 and 4.5706/6.9053 units respectively in scaled DFT.

C=C stretching vibrations are generally occur in the range 1680cm^{-1}-1630cm^{-1} [26], here they were were calculated at 1624cm^{-1}, 1483cm^{-1}, 1149 cm^{-1} with Raman activity/IR intensity 26.1030/3.1803, 81.2979/103620, 14.0403/1161.2000 units in scaled DFT. C-O stretching vibrations were recorded at 1185cm^{-1},1149cm^{-1}, 1099cm^{-1}, 1033cm^{-1}, 900cm^{-1}, 349cm^{-1} with Raman activity/IR intensity 6.9571/7.0379, 14.0403/1161.2000, 2.2426/7.7562, 7.9910/4.3749, 3.8238/22.8930, 8.0452/9.5009 units respectively. Ring deformation vibrations were recorded below 1275cm^{-1} and ring torsion vibrations were recorded below 762 cm^{-1}. In plane bending vibrations of C-C were calculated at 417cm^{-1}, 398cm^{-1}, 360cm^{-1}, 238cm^{-1}, 189cm^{-1}, 169cm^{-1} and 95cm^{-1} with Raman activity/IR intensity 2.6913/1.9238, 0.8150/11.8220, 2.2902/0.2448, 1.6805/2.8926, 1.9258/7.6907, 2.6937/6.0628 and 0.7279/3.4596 units respectively. Similarly, out of plane bending of C-C bending vibrations were recorded at 691cm^{-1}, 671cm^{-1}, 417cm^{-1}, 398cm^{-1}, 360cm^{-1},238cm^{-1}, 189cm^{-1}, 159cm^{-1} and 95cm^{-1} with Raman activity/ IR intensity 0.2901/23.9430, 6.4753/11.0880, 2.6913/1.9238, 0.8150/11.8220, 2.2902/0.2448, 1.6805/2.8926, 1.9258/7.6907, 2.6937/6.0628 and 0.7279/3.4596 units, respectively.

3.2.2 CH_2 vibration

Literature reviews suggest that the asymmetric stretching of CH_2 occurs in the region 3000cm^{-1}-2800cm^{-1} whereas symmetric stretching occurs in the region 2900cm^{-1} -2800 cm^{-1} [27], but here symmetric stretching of CH_2 (pure mode) was recorded at 2900cm^{-1} with Raman Activity/IR intensity 89.7099 and 59.2930 units respectively. Remaining CH_2 stretching vibrations were calculated at 2916cm^{-1}, 2941cm^{-1} and 2961cm^{-1} with Raman activity/ IR intensity 114.0720 /40.3970, 50.4533/27.4440 and 59.6634/ 16.7150 units, respectively. Moreover, bending, wagging, twisting and rocking were recorded below 1520cm^{-1}, 1455 cm^{-1}, 1304cm^{-1} and 1149 cm^{-1}respectively.

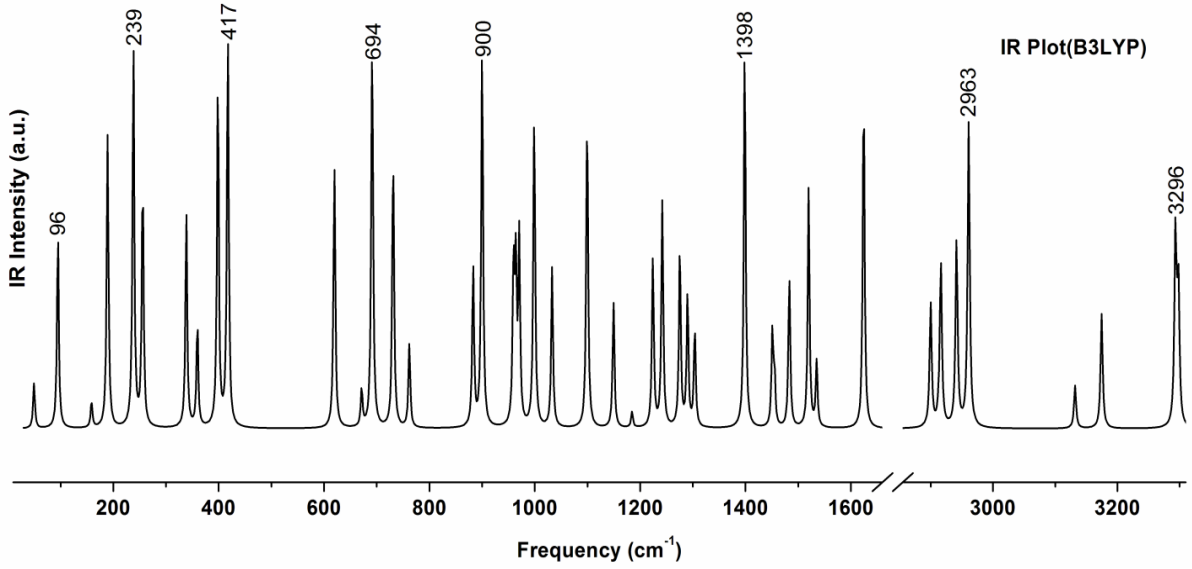

Fig. 2: IR spectra of BHMF between the ranges 10 —3310 cm^{-1} (Intensity of selected characteristic modes are assigned).

3.2.3 OH vibration

The non-hydrogen bonded or free hydroxyl group absorbs strongly in the region 3600cm^{-1}-3550cm^{-1} whereas the existence of hydrogen bond can lower the O-H stretching wave number to 3550cm^{-1}-3200cm^{-1} region with an increase in IR intensity and breadth [28]. The in-plane deformation vibrations appear strong in the region 1440cm^{-1}-1260 cm^{-1} [29]. Here, there are two O-H groups and their symmetric stretching vibrations were recorded at 3519cm^{-1} and 3656 cm^{-1} with Raman activity/ IR activity 242.7130/ 5.4531 and 234.4250/ 3.3227 units respectively. All the C-C and CHO deformations were recorded below 1455 cm^{-1}.

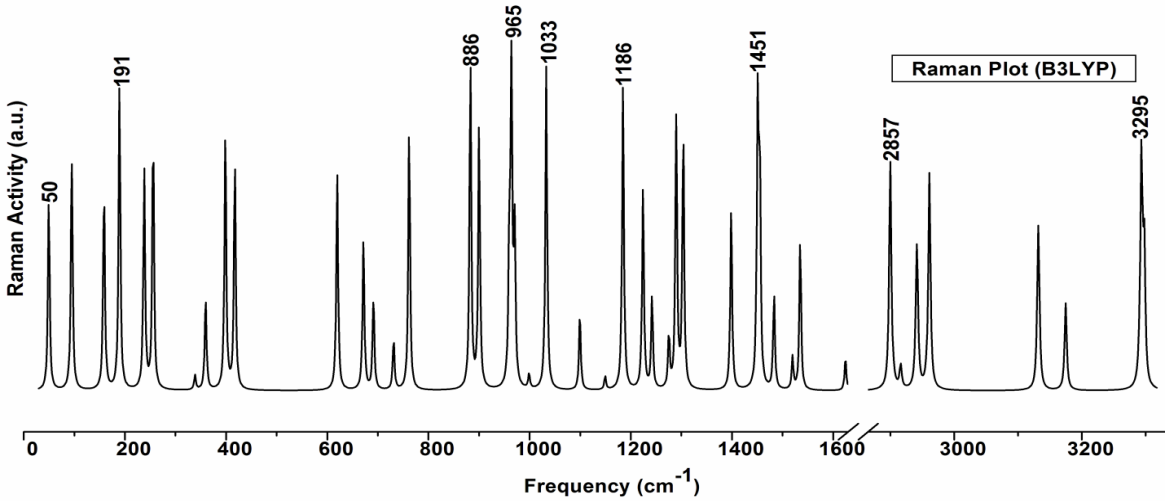

Fig. 3: Raman spectra of BHMF between the ranges 0 —3310 cm^{-1} (Intensity of selected characteristic modes are assigned).

3.3 Electronic Properties

3.3.1 Mulliken Atomic Charges

Mulliken atomic charges are useful in determining the chemical reactivity of compounds. The Mulliken charges for BHMF are listed in the Table 3. From the table, C9 has the highest positive charge of all carbon atoms and are thus predicted to be the target of nucleophilic attack. Also, the oxygen atom O1 has a positive charge and rest two oxygen atoms have negative charges as shown in Fig. 4. All the hydrogen atoms are associated with positive charges.

Table 3: Mulliken charges for BHMF.

Atoms	Mulleken atomic charges
O1	0.507734
O2	-0.554525
O3	-0.554760
C4	-0.003856
C5	0.367248
C6	-0.214200
C7	-0.230092
C8	-0.206398
C9	0.082129
H10	0.180081
H11	0.184916
H12	0.188372
H13	0.197543
H14	0.190897
H15	0.211978
H16	0.333533
H17	0.334868

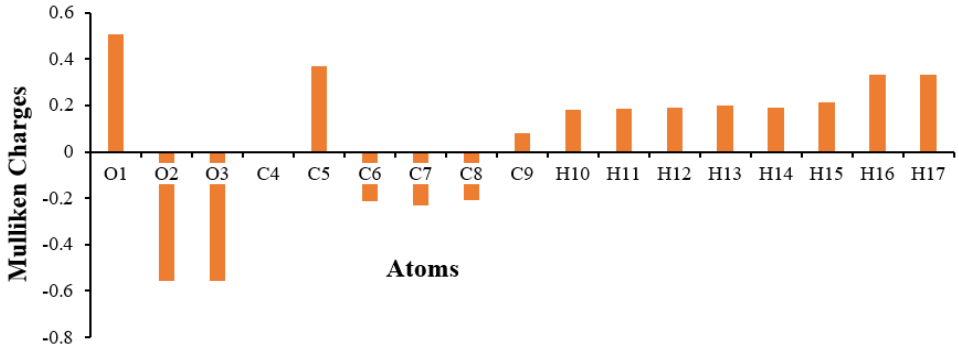

Fig. 4: Mulliken charge plot of BHMF.

3.3.2 Molecular Electrostatic Potential Surface (MESP)

The MESP provides a visual method to understand the relative polarization of molecule [30]. In the surface generated, negative electrostatic potential (shades of red color) corresponds to an attraction of the proton by the concentrated electron density in the molecules and positive electrostatic potential (shades of blue

color) corresponds to repulsion of the proton. The largely white or lighter yellow color shades on the surface indicate that the molecule is mostly non-polar. In the surface generated the deepest red region around the oxygen atoms is global negative site and is favorable for the electrophilic attack. Whereas, the deepest blue regions around the hydrogen atoms are the global positive site and is favorable for nucleophilic attack. The positive potential increases in the order red < orange < yellow <green (Fig. 5). The bonding of any molecule with other molecules depends upon the charge distributions around the molecule. So, MESP play an important role to identify the bonding sites of molecule biologically.

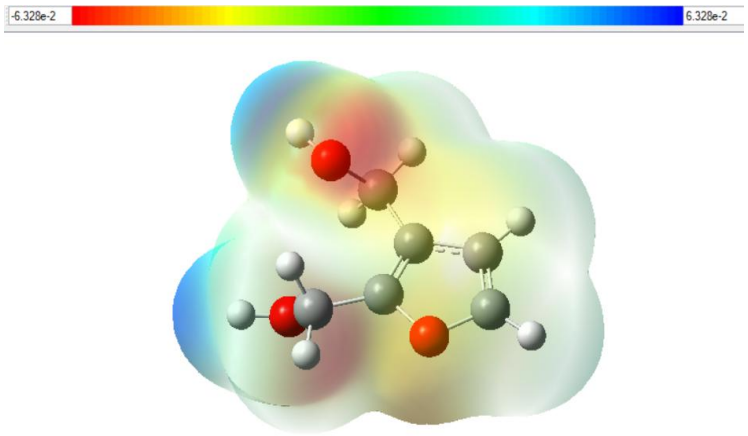

Fig. 5: Molecular electrostatic potential mapped on isogeneity surface in the range -6.328× 10^{-2}(red) to 6.328× 10^{-2}(blue) for BHMF.

3.3.3 UV-Visible spectra

UV-Vis is a spectroscopy which involves the interaction of ultraviolet and visible radiations with matter. It is an analytical technique that measures the number of discrete wavelengths of UV or visible light that are absorbed by or transmitted through a sample [30]. In order to plot the UV-Vis spectra, time dependent density functional theory (TD-DFT) calculations were performed in both gaseous phase as well as solvent (ether) environment. Theoretically plotted UV-Vis absorption spectra are shown in the Figs. 6 and 7 respectively corresponding to gaseous phase and solvent phase.

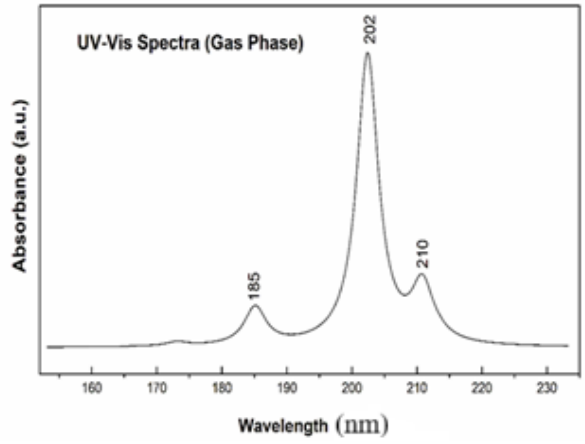

Fig. 6: UV-Vis plot of BHMF in gas phase between the ranges 160-230 cm^{-1}. Sigle peak with the highest absorbance was assigned and it was observed at 202cm^{-1}.

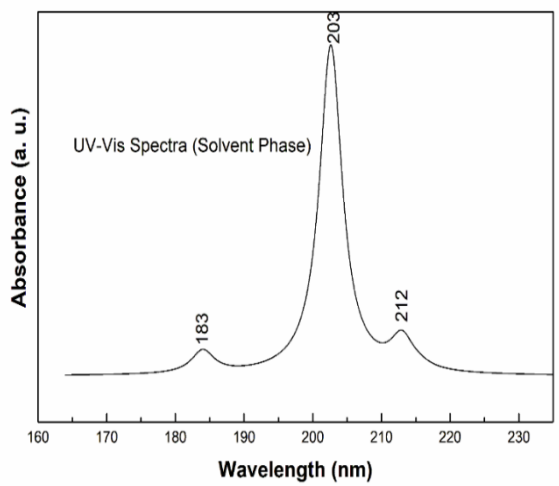

Fig. 7: UV-Vis plot of BHMF in solvent (Eather) phase between the ranges 160-230 cm^{-1}. Sigle peak with the highest absorbance was assigned and it was observed at 203cm^{-1}.

3.4 Physicochemical Properties

Its molar refractivity (30.96) indicates its low polarizability, which is characteristic of the compact aromatic core. Thus, together these descriptors suggest a molecule of suitable polarity (for aqueous solubility) and lipophilicity (for passive absorption), consistent with the physicochemical requirements for oral bio-availability agents. Physicochemical properties of the title compound calculated by the Swiss ADMDE web tool are shown in Table 4.

Table 4: Physicochemical Properties of BHMF.

Physicochemical Properties	
Formula	$C_6H_8O_3$
Molecular weight	128.13 g/mol
Num. heavy atoms	9
Num. arom. heavy atoms	5
Fraction Csp3	0.33
Num. rotatable bonds	2
Num. H-bond acceptors	3
Num. H-bond donors	2
Molar Refractivity	30.96
TPSA	53.60 Å²

3.4.1 Lipophilicity

The title compound possesses low lipophilicity (consensus LogP = 0.07). Calculated from 3D models, predictions range from −0.97 to +1.20; consensus is about neutrality between hydrophilic and lipophilic tendencies. This balanced value of lipophilicity is favorable for oral absorption, distribution and formulation flexibility. However, its low lipophilicity might restrict its ability to penetrate through very lipophilic barriers such as the blood–brain barrier, restricting its therapeutic uses in peripheral targets. The title compound's lipophilicity is displayed Table 5.

Table 5: Lipophilicity of BHMF.

Lipophilicity	
Log $P_{o/w}$ (iLOGP)	1.20
Log $P_{o/w}$ (XLOGP3)	-0.75
Log $P_{o/w}$ (WLOGP)	-0.04
Log $P_{o/w}$ (MLOGP)	-0.97
Log $P_{o/w}$ (SILICOS-IT)	0.94
Consensus Log $P_{o/w}$	0.07

3.4.2 Pharmacokinetics

Furandimethanol is highly absorbed in the gastrointestinal track but not across the blood–brain barrier. it is not P-glycoprotein substrate, and do not inhibit important CYP450 isoenzymes (CYP1A2, CYP2C19, CYP2C9, CYP2D6, and CYP3A4). The skin penetration coefficient (Log Kp = −7.61 cm/s) is indicative of low dermal absorption. The present characteristics support its potential as an orally administrable, but not a CNS-available drug. The lack of CYP450 inhibition decreases its potential for drug–drug interactions, adding to the safety profile.
Pharmacokinetics of title compound are presented in Table 6.

Table 6: Pharmacokinetics of BHMF.

Pharmacokinetics	
GI absorption	High
BBB permeant	No
P-gp substrate	No
CYP1A2 inhibitor	No
CYP2C19 inhibitor	No
CYP2C9 inhibitor	No
CYP2D6 inhibitor	No
CYP3A4 inhibitor	No
Log K_p (skin permeation)	-7.61 cm/s

3.4.3 Drug-likeness

Numerous parameters including molecular weight, hydrogen bond acceptors and donors, molar refractivity, polar surface area, number of rotatable bonds, and ALogP were accessed to study the drug-likeness of the title molecule using Swiss ADMDE web tool. The compound also satisfies all the descriptors of Lipinski's Rule of Five [31] and Veber–Egan filters. But it violated Ghose filter (small size and low molar refractivity) and Muegge's rule (molecular weight >200). The low score of 0.55 suggests moderate yet satisfactory oral bioavailability. Furandimethanol adheres to the basic principles of drug-likeness however its size may be limiting target engagement and metabolic stability, likely requiring structural elaboration during optimization. The result is summarized in Table 7.

Table 7: Drug-likeness Properties of BHMF.

Drug-likeness	
Lipinski	Yes; 0 violation
Ghose	No; 3 violations: MW<160, MR<40, #atoms<20
Veber	Yes
Egan	Yes
Muegge	No; 1 violation: MW<200
Bioavailability Score	0.55

3.4.4 Medicinal Chemistry

No PAINS (Pan-Assay Interference Compounds) and Brenk alerts were observed, thus excluding any false positive or structural toxicity liabilities. It synthetic accessibility (SA) score of 2.50 (on a scale from 1 to 10) shows the relative ease of its chemical synthesis. However, the molecule does not satisfy the stringent "lead-like" criteria, and that is essentially because it has a low molecular weight (<250). Thus, Medicinal chemistry-wise, furandimethanol was a chemically suitable and non-toxic moiety that could be a potential drug hit or lead precursor despite not being fully optimized in its own right (Fig.8).

Furandimethanol sits in the borderland between being a fragment and sometimes being described as a highly soluble molecule, benignly oriented from a pharmacokinetic standpoint.

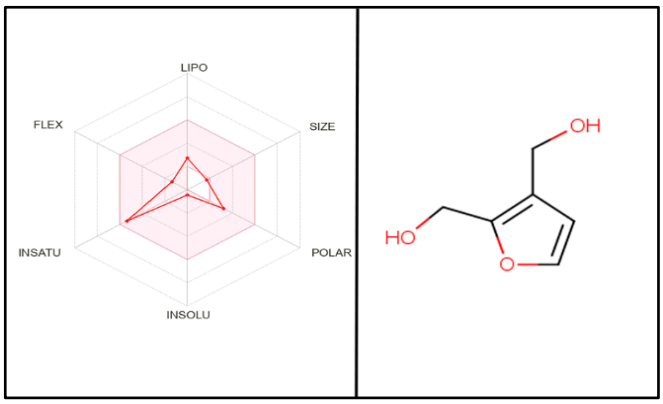

Fig. 8: Radar Plot and Molecular structure retrived from SWISS ADME web tool.

Table 8: medicinal chemistry of BHMF.

Medicinal Chemistry	
PAINS	0 alert
Brenk	0 alert
Lead likeness	No; 1 violation: MW<250
Synthetic accessibility	2.50

The physicochemical balance favors oral absorption. Meanwhile, its aqueous solubility and metabolic safety profile fit irony as such may further attract it to early drug discovery. The only limitations stem essentially from a somewhat diminutive molecular framework, which greatly reduces its applicability for high-affinity target binding and CNS applicability. Hence, Furandimethanol is better served in being considered a candidate for fragment-to-scaffold development than as a final therapeutic. Medicinal chemistry of title compound is presented in Table 8.

3.5 Molecular Docking

Molecular docking approach is a computer-aided technique to predict protein-ligand interaction of a drug molecule. It predicts biding modes as well as binding affinity of ligand with target proteins which plays key role in drug design [7,8, 32]. This study aims to assess inhibitory activity and binding interactions and reactive sites on a single protein. The proteins with code 1S5B was retrieved from protein data bank to conduct molecular docking with BHMF [33]. The active sites of the protein have been predicted by removing water molecules within a grid box of size 20Å×20Å×20Å and grid box spacing 0.375Å. Blind docking approach has been adopted with all the six protein chains collectively because the active site of the molecule is unspecified and unknown. The docking result according to the estimations made by AutoDock Vina with different parameters like the conventional hydrogen bond lengths, inhibition constant, binding affinity, and RMSD of the docked structure of the ligand and selected proteins are displayed in table 9. Different ligand binding mechanisms are associated with proteins that have the lowest binding affinities. AutoDock Vina gives nine different ligand binding mechanisms. Table 9 represents binding mechanism associated with proteins that has the lowest binding affinities. The results of docking are interpreted in terms of conventional hydrogen bonding as they can specify complementary groups in protein binding sites and are responsible to influence the ligand's binding orientation by contributing overall binding affinity [34]. The Ramachandran plot, Protein structure, docked complex with best-fit Pose are displayed in the Figs 9, 10 and 11, respectively.

Table 9: Docking result.

Selected PDB code and their resolution	Binding Affinity (kcal/ mol)	H-Bond residues	Atoms	Bond length (Å)	Ligand efficiency	Inhibition constant (µM)	RMSD l.b.(Å)	RMSD u.b.(Å)
		THR F :78	H17	2.17				
1S5B	-5.2	THR F :78	O3	2.19				
(2.13 Å)		ARG A : 148	O1	2.47	-0.57	153	0.00	0.00

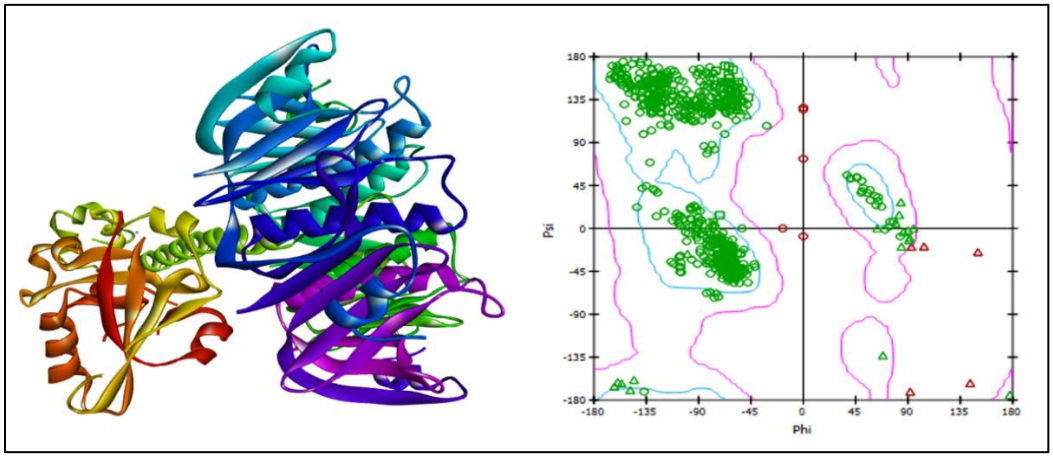

Fig. 9: The Ramachandran plot.

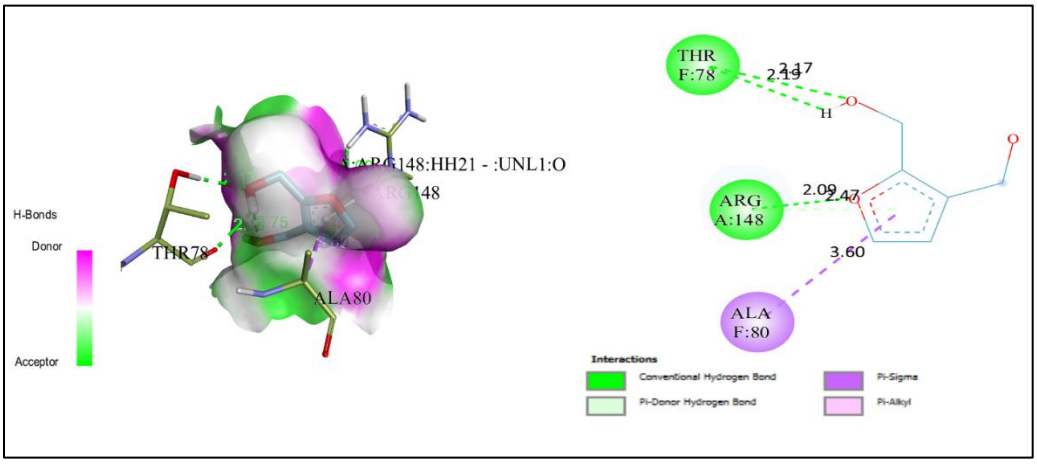

Fig. 10: Docked complex 3D and 2D with best-fit Pose

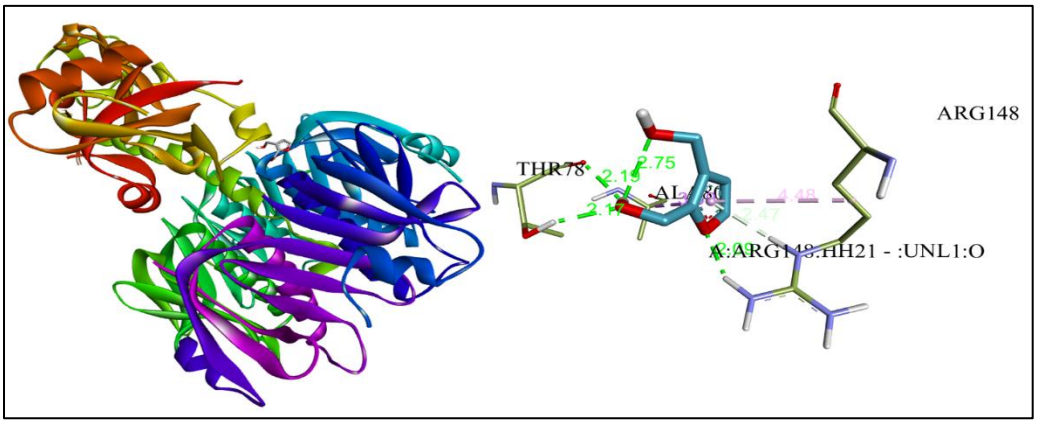

Fig. 11: Docked complex 3D and 2D with best-fit Pose.

3.5.1 Docking of BHMF with 1S5B

1S5B (2.13 Å resolution) is the mutant cholera holotoxin from *Vibrio cholerae*. It Is a six-chain protein. It consists of one enzymatic A-subunit and five receptor-binding B-subunits (AB_5 toxin complex). This mutant provides key information to researchers to understand the activation mechanism of cholera toxin and its role in disease [35]. Active binding sites of protein code 1S5B were confirmed within a grid box, centered at center x = 58.121841, y = -43.059349, and z = 48.058959 run Vina with 8 exhaustiveness. The binding affinity is –5.2 kcal/mol, with an inhibition constant of 153 µM and ligand efficiency -0.57. The RMSD l.b and RMSD u.b between the docked and starting structure are 0.00 Å respectively. The hydrogen bonds of residues THR F :78 and THR F :78 are formed with atoms H17, O3 and O1 having bond lengths 2.17, 2.19 and 2.47 Å, respectively. Having greater inhibition constant and RMSD with a lower negative value of binding affinity BHMF is a moderator inhibitor of 1S5B.

4. CONCLUSIONS

The geometrical parameters, bond length, bond angles, dihedral angles and harmonic vibrational wavenumbers of all the 45 normal modes of the furandimethanol were determined and analyzed at DFT/B3LYP/6-31g. The longest and the shortest bond length for the title compound were found 1.474Å and 0.972Å in between C4-C6 and O-H respectively. The highest and lowest bond angles were found between C7-C9-H15 and C5-C4-C7 with respective values 133.80° and 106.12°. The lowest to highest dihedral angles in clockwise directions were found in the range 0.01°-179.96°, whereas the lowest to highest dihedral angles in counter-clockwise direction were found in the range 0.00°-179.99°. The IR and the Raman spectra were presented, and the vibrational bands were assigned with IR intensity and Raman activity on the basis of the PED obtained from the DFT calculations and plot of molecular electrostatic potential (MEP) and UV-Vis spectra have been plotted and presented. From the analysis of IR and Raman spectra it as found that the molecule is both IR and Raman active. Physicochemical properties, lipophilicity, drug-likeness, medicinal chemistry and molecular docking have been studied and analyzed. The balanced lipophilicity and excellent water solubility for title molecule are significantly advantageous in drug development because they are favorable for oral absorption, distribution and formulation flexibility. Furandimethanol meets the basic principles of drug-likeness. However, its small size and lack CYP450 inhibition decreases its potential for drug–drug interactions, that adds the safety profile and may be limiting target engagement and metabolic stability, likely requiring structural elaboration during optimization. The molecular docking of tilte molecule with IS5B suggests that having greater inhibition constant and RMSD with a lower negative value of binding affinity, it is a moderator inhibitor of 1S5B. So Furandimethanol has great importance in chemistry, biology,

pharmacology, medicinal chemistry and drug designing fields and the output of this work will be employed as basic information regarding to molecule used accordingly in respective fields mentioned earlier. The information drawn from this work helps for the further research on the title molecule.

AUTHORS CONTRIBUTION

All authors contributed equally to the conception, data analysis, and writing of the manuscript.

ETHICAL STATEMENT

The present study is entirely based on computational and theoretical analyses, including quantum chemical calculations, molecular docking, and pharmacokinetic predictions. No human participants, animals, or biological samples were involved in the research. The authors affirm that the work complies with standard publication ethics and contains no fabrication, falsification, or plagiarism.

CONFLICT OF INTEREST

The authors declare that they have no known competing financial interests or personal relationships that could have appeared to influence the work reported in this paper.

ACKNOWLEDGMENTS

The authors gratefully acknowledge to Prof. Dr. Bhawani Datt Joshi for fruitful suggestions and guidance during research period. Our sincere acknowledgement goes to Prof. Poonam Tandon, DDU, Gorakhpur, India for providing software facilities. Also, we thank to the Department of Physics, Siddhanath Science Campus, Mahendranagar, Kanchanpur**,** T.U, for providing computational lab facilities.

REFERENCES

[1] A. Kumar, MD. N. Sarker and S. Paul, The thermo physical, HOMO, LUMO, Vibrational spectroscopy and QSAR study of morphonium formate and acetate Ionic Liquid Salts using computational method*, Turkish Comp. Theo. Chem.*, **3** (2019) 59-68. https://doi.org/10.33435/tcandtc.481878

[2] S.L. Dhonnar, N.V. Sadgir, V.A. Adole and B.S. Jagdale, Molecular Structure, FT-IR Spectra, MEP and HOMO-LUMO Investigation of 2-(4-Fluorophenyl)-5-phenyl-1, 3,4-oxadiazole Using DFT Theory Calculations*, Advanced Journal of Chememistry A*, **4** (2021) 220-230. https://dx.doi.org/10.22034/ajca.2021.283003.1254

[3] **V**.A. Adole, Synthesis; Antibacterial, Antifungal and DFT studies on structural, electronic and chemical reactivity of (E)-7-(ClH-Indole-3yl)methylene-1,2,6,7-tetrahydro-8H-indeno[5,4-B]Furan-8-one, *Advanced Journal of Chemistry A*, **4**(2021) 175-187. https://dx.doi.org/10.22034/ajca.2021.278047.1250

[4] http//en.wikipedia.org/wiki/2,5 bis(hydroxymethyle)furan. Accessed on 2022/01/10.

[5] B.D. Joshi, P. Tandon, S. Jain, Structure, MESP and HOMO-LUMO study of 10-Acetyl-10H-phenothiazine 5-oxide using vibrational spectroscopy and quantum chemical methods, *BIBECHANA*, **9** (2013) 38-49. https://doi.org/10.3126/bibechana.v9i0.7151.

[6] M. Yadava, Shivani, A. Ahamada, K.K. Singha, R. Singha, A. Misraa, P. Tandon, *ab*-Initio and DFT study of HCN: Role of temperature for the formation of HCN molecule in the interstellar medium*, Journal of Molecular Structure,* **1248** (2022) 131460. https://doi.org/10.1016/j.molstruc.2021.131460.

[7] M. Chaudhary, K. Tyagi, A review on molecular docking and its application *International Journal of Advanced Research* (Mar), **12** (2024) 1141-1153. http://dx.doi.org/10.21474/IJAR01/18505.

[8] G.B. Dhami, M.R. Bhatt, S.R. Joshi, B.D. Joshi, First Principle Study on Structural, Electronic, Vibrational Properties and Molecular Docking Study of Tyramine. *KMC Journal*, **5** (2023) 241-260. https://doi.org/10.3126/kmcj.v5i2.58241

[9] Pubechem Database: *https://pubchem.ncbi.nlm.nih.gov/compound/structure search*. Accessed on 2/1/2022.

[10] B.D. Joshi, G. Thakur, M.K. Chaudhary, Molecular structure, HOMO-LUMO and vibrational analysis of Ergoline by using Density Functional Theory, *Scientific world,* **14** (2021) 21-30. http://doi.org/10.3126/sw.v14.34978

[11] A. Ignaczak, O.Łukasz, In search of the most stable molecular configuration of heptakis (2, 6-O-dimethyl)-β-cyclodextrin and its complex with mianserin: A comparison of the B3LYP-GD2 and M062X-GD3 results, *The Journal of Physical Chemistry B*, **48** (2021) 13077-13087. https://doi.org/10.1021/acs.jpcb.1c06831.

[12] M.J. Frisch, G.W. Trucks, H.B. Schlegel. G.E. Scuseria, J.R. Cheeseman, M.A. Robb, G. Scalmani, V. Barone, B. Mennucci, G.A. Petersson, H. Nakatsuji, M. Caricato, X. Li, H.P. Hratchian, A.F. Izmzylov, J. Bloino, G. Zheng, J.L. Sonnenberg, M. Hada, M. Ehara, K. Toyota, R. Fukuda, J. Ishida, M. Hasegawa, T. Nakajima, Y. Honda, O. Kitao, H. Nakai, T. Vreven, J.A. Montgomery Jr., J.E. Peralta, F. Ogliaro, M. Bearpark, J.J. Heyd, E. Brothers, K.N. Kudin, V.N. Staroverov, R. Kobayashi, J. Normand, A. Raghavachari, A. Rendell, J.C. Burant, S.S. Iyengar, J. Tomasi, M. Cossi, N. Rega, J.M.Millan, M. Klene, J.E. Knox, J.B. Cross, V. Bakken, C. Adamo, J. Jaramillo, R. Gomperts,R.E. Stratmann, O. Yazyev, A.J. Austin, R. Cammi, C. Pomelli, J.W. Ochterski, R.L. Martin, K. Morokuma, V.G. Zakrzewski, G.A. Voth, P. Salvador, J.J. Dannerberg, S. Dapprich, A.D. Daniels, J. Farkas, B. Foresman, J.V. Ortiz, J. Cioslowski, D.J. Fox, *GAUSSIAN 09, Revision, Gaussian, Inc., Wallingford CT*, (2010).

[13] D. Bálint, L. Jäntschi, Comparison of molecular geometry optimization methods based on molecular descriptors, *Mathematics*, ***9*** (2021) 2855. https://doi.org/10.3390/math9222855.

[14] B. Miehlich, A. Savin, H. Stoll, H. Preuss, Results obtained with the correlation energy density functionals of Becke and Lee, Yang and Parr, *Chemical Physics Letters*, ***157*** (1989) 200-206. https://doi.org/10.1016/0009-2614(89)87234-3.

[15] R. G. Parr, W. Yang, Density Functional Theory of atoms and molecules*,* Oxford University press, New York, Oxford, (1989). https://doi.org/10.1002/qua.560470107

[16] J.M.L. Martin, C.V. Alsenoy, *Gar2ped*, University of Antwerp, 1995.

[17] R. Bulín, M. Hajžman, P. Polach, Nonlinear dynamics of a cable–pulley system using the absolute nodal coordinate

formulation, *Mechanics Research Communications*, **82** (2017) 21-28. https://doi.org/10.1016/j.mechrescom.2017.01.001.

[18] O. Daina, V.Z. Michielin, Swiss ADME: a free web tool to evaluate pharmacokinetics, drug-likeness and medicinal chemistry friendliness of small molecules, *Scientific Report,* **7** (2017), 42717. https://doi.org/10.1038/srep42717

[19] O. Trott, A. J. Olson, AutoDock Vina: Improving the Speed and Accuracy of Docking with a New Scoring Function, Efficien Optimization and Multithreading, *Journal of Computational Chemistry*, **31** (2010) 455-461. https://doi.org/10.1002/jcc.21334

[20] G.M. Morris, R. Huey, W. Lindstrom, M.F. Sanner, R.K. Belew, D.S. Goodsell, AutoDock4 and AutoDock Tools4: Automated Docking with Selective Receptor Flexibity. *Journal of Computational Chemistry*, 30 (2009) 2785–2791. https://doi.org/10.1002/jcc.21256

[21] D. Systemes, BIOVIA Discovery Studio Dassault Systmes (2016). https://www.3ds.com/products/biovia/discovery-studio

[22] L.L.C. Schrödinger, D.W. PyMOl, The PyMOL Molecular Graphics System, Version 2.5.4. (2020). https://www.pymol.org.

[23] Protein Data Bank (RCSB), https://www.rcsb.org.

[24] N.M. O'Boyle, M. Banck, C.A. James, C. Morley, T. M. Vander, G.R. Hutchison, Open Babel: an open chemical toolbox. J Cheminform. **3** (2011) 33. https://doi.org/10.1186/1758-2946-3-33

[25] *https://www.google.com/c-c bond length search*. Accessed on 10/1/2022.

[26] B.D. Joshi, G. Thakur, M.K. Chaudhary, Molecular structure, HOMO-LUMO and vibrational analysis of Ergoline by using Density Functional Theory, *Sci. world,* **14** (2021) 21-30. http://doi.org/10.3126/sw.v14.34978.

[27] P. Pulay, G. Fogarasi, F. Pang, J.E. Boggs, Systematic *ab initio* gradient calculation of molecular geometries, force constants, and dipole moment derivatives, *Journal of American Chemical Society,* 101 (1979) 2550-2560. https://doi.org/10.1021/ja00504a009.

[28] D.L. Vein, N.B. Clotthup, W.G. Fately, J.G. Grasselli, The handbook of infrared and Raman characteristic frequencies of organic molecules, *Academic Press Inc, San Diego California*, (1991).

[29] E.F. Mooney, The chemical infrared spectra of chlorobenzene and bromobenzene derivatives-III Tolunes*, Spect.chem. Acta,* **20** (1964) 1343-1348. https://doi.org/10.1016/0371-1951(64)80114-4

[30] K. Srishailam, L. Ravindranath, B.V. Reddy, G.R. Rao, Electronic spectra (experimental and simulated), and DFT investigation of NLO, FMO, NBO, and MESP characteristics of some Biphenylcarboxaldehydes, *Polycyclic Aromatic Compounds*, **8** (2023) 7200-7213. https://doi.org/10.1080/10406638.2022.2130376

[31] C.A. Lipinski, F. Lombardo, B.W. Dominy, P.J. Feeney, Experimental and computational approaches to estimate solubility and permeability in drug discovery and development settings, *Adv. Drug Deliv. Rev*, **46** (2001) 3–26. https://doi.org/10.1016/S0169-409X(00)00129-0.

[32] M.K. Chaudhary, A. Srivastava, A.K. Singh, P. Tondon, B.D. Joshi, Computational evaluation on molecular stability, reactivity, and drug potential of frovatriptan from DFT and molecular docking approach, *Computational and Theoretical Chemistry*, **1191** (2020) 113031. https://doi.org/10.1016/j.comptc.2020.113031.

[33] P.W. Rose, B. Beran, W.F. Bluhm, C. Bi D. Dimitropoulos, D.S. Goodsell, A. Prlic, M. Quesada, G.B. Quinn, J.D. Westbrook, J. Young, B. Yukich, C. Zardecki, H.M. Berman, P.E. Bourne, The RCSB protein data bank: redesigned web site and web services, *Nucleic Acids Res.* **39** (2011) D392–D401. https://doi.org/10.1093/nar/gkq1021.

[34] M. Meyer, P. Wilson, D. Schomburg, Hydrogen bonding and molecular surface shape complementarity as a basis for protein docking, *Journal of Molecular Biology,* **264** (1996) 199–210. https://doi.org/10.1006/jmbi.1996.0634.

[35] C.J. O'Neal, E. I. Amaya, M. G. Jobling, R. K. Holmes, W. G. Hol, Crystal structures of an intrinsically active cholera toxin mutant yield insight into the toxin activation mechanism, *Biochemistry,* **43** (2004) 3772-3782. https://doi.org/10.1021/bi0360152.